2018-01-1493 Published 13 Jun 2018

Computational Aeroacoustics Based on a Helmholtz-Hodge Decomposition

Manfred Kaltenbacher and Stefan Schoder Vienna University of Technology

Citation: Kaltenbacher, M. and Schoder, S., "Computational Aeroacoustics Based on a Helmholtz-Hodge Decomposition," SAE Technical Paper 2018-01-1493, 2018, doi:10.4271/2018-01-1493.

Abstract

Using existing aeroacoustic wave equations, we propose a general hybrid aeroacoustic method, based on compressible flow data. By applying the Helmholtz-Hodge decomposition on arbitrary domains, we extract the incompressible projection (non-radiating base flow) of the compressible flow velocity by solving the vector valued curl-curl equation with the vorticity as forcing term. The resulting vortical flow part is used for computing the acoustic source term. This method maintains the favorable properties of the hybrid aeroacoustic method, while still considering acoustic feedback on the flow field.

Introduction

In modern transport systems, passengers' comfort is greatly influenced by flow induced noise. The cavity with a lip represents a generic model of a vehicle door gap, involving an acoustic feedback mechanism on the underlying flow field. Even though, great advances have been made in direct computation of aerodynamic sound, a Direct Numerical Simulation with commercial solvers, fully resolving flow and acoustic quantities is infeasible for most practical applications. However, the classical hybrid approach, of first performing an incompressible flow computation, evaluate the acoustic sources and finally compute the acoustic field does not consider any feedback of the acoustic field on the flow (see, e.g., [1, 2, 3]). Therefore, we propose the following approach: (1) Perform a compressible flow simulation, which incorporates two-way coupling of flow and acoustics; (2) Filter the flow data by the Helmholtz-Hodge decomposition, such that we obtain a pure non-radiating field with which the acoustic sources are computed; (3) Perform the acoustic propagation computation. Our approach is of strong practical relevance, since state of art commercial flow solvers are just second order accurate in space and time and do not provide a computational boundary treatment, which is capable to absorb both vortices and waves without reflections. Computations of the aeroacoustic benchmark case, cavity with a lip [4], involving acoustic feedback show promising results and demonstrate the applicability of our approach.

Aeroacoustic Formulation

A general acoustic analogy composes a hyperbolic left hand side defined by a wave operator $\Box$ and a generic right hand side **RHS**($\star$)

$$\Box p' = \mathrm{RHS}\left(p, \boldsymbol{u}, \rho, \ldots\right). \tag{1}$$

To this end, Lighthill's inhomogeneous wave equation perfectly fits to this class, which reads as [5, 6].

$$\frac{\partial^2 \rho'}{\partial t^2} - c_0^2 \nabla \cdot \nabla \rho' = \nabla \cdot \nabla \cdot \left[T\right]. \tag{2}$$

In (2) ρ' denotes the density fluctuation, c_0 the constant speed of sound and the entries of the Lighthill tensor $[\boldsymbol{T}]$ compute by

$$\left[T\right] = \rho \boldsymbol{u}\boldsymbol{u} + \left(\left(p - p_0\right) - c_0^2\left(\rho - \rho_0\right)\right)\left[I\right] - \left[\tau\right] \tag{3}$$

with the fluid velocity $\boldsymbol{u}$, the pressure and density fluctuations $p' = p - p_0$, $\rho' = \rho - \rho_0$ and the viscous stresses $[\boldsymbol{\tau}]$. It is obvious that the right hand side **RHS**($\star$) of Lighthill's inhomogeneous wave equation contains not only source terms, but also nonlinear and interaction terms between the sound and flow field, which includes effects such as convection and refraction of the sound by the flow. Therefore, the whole set of compressible flow dynamics equations have to be solved in order to calculate the right hand side of (2). However, this means that we have to resolve both the flow structures and acoustic waves, which is an enormous challenge for any numerical scheme and the computational noise itself may strongly disturb the physical radiating wave components [1]. Therefore, in the theories of Phillips and Lilley interaction effects have been, at least to some extent, moved to the wave operator $\Box$ [7, 8]. These equations predict certain aspects of the sound field surrounding a jet quite accurately, which are not accounted for Lighthill's equation due to the restricted numerical resolution of the source term in (2) [9].

In 2003, Goldstein proposed a method to split flow variables $(p, \boldsymbol{u}, \ldots)$ into a base flow (non-radiating) and a remaining component (acoustic, radiating fluctuations) [10].

$$\star = \tilde{\star} + \star'. \tag{4}$$

Applying the decomposition to the right hand side of the wave equation (the left hand side of the equation is already treated in this manner during the derivation of the acoustic analogy) leads to

$$\Box p' = \mathrm{RHS}\left(\tilde{p},\tilde{u},\tilde{\rho},p',u',\rho',\ldots\right). \tag{5}$$

Now interaction terms can be moved to the differential operator to take, e.g., convection and refraction effects into account, and even nonlinear interactions can be considered. Therefore, we propose the three steps to relax the Mach number constraint imposed by the incompressible flow simulation:

1. Perform a compressible flow simulation, which incorporates two-way coupling of flow and acoustics.
2. Filtering of the flow field, such that we obtain a pure non-radiating field from which we compute the acoustic sources.
3. Solve with an appropriate wave operator for the radiating field

$$\Box p' = \mathrm{RHS}\left(\tilde{p},\tilde{v},\tilde{\rho},\ldots\right). \tag{6}$$

The non-radiating base flow is obtained by applying a Helmholtz-Hodge decomposition (see Sec.). For the computation of the wave propagation, we apply the equation of vortex sound [11] based on the total enthalpy

$$H = \int \frac{\mathrm{d}p}{\rho} + \frac{u^2}{2} \tag{7}$$

as primary variable, with $u^2 = \boldsymbol{u}\cdot\boldsymbol{u}$. The acoustic analogy for homentropic flow reads as

$$\frac{1}{c^2}\frac{\mathrm{D}^2}{\mathrm{D}t^2}H - \nabla\cdot\nabla H = \nabla\cdot\left(\boldsymbol{\omega}\times\boldsymbol{u}\right) = \nabla\cdot\boldsymbol{L}\left(\boldsymbol{u}\right), \tag{8}$$

where for a constant isentropic speed of sound c and density ρ_0 the equation demonstrates the relevancy of the vorticity as aeroacoustic source term. The wave operator is of convective type, where the total derivative (material derivative) is defined as $\frac{\mathrm{D}\star}{\mathrm{D}t} = \frac{\partial\star}{\partial t} + \left(\boldsymbol{u}\cdot\nabla\right)\star$. The aeroacoustic source term is known as the divergence of the Lamb vector $\boldsymbol{L}$

$$\boldsymbol{L}\left(\boldsymbol{u}\right) = \left(\boldsymbol{\omega}\times\boldsymbol{u}\right). \tag{9}$$

In our formulation, the Lamb vector in terms of the non-radiating base flow $\tilde{\boldsymbol{u}}$ reads as follows

$$\boldsymbol{L}\left(\tilde{\boldsymbol{u}}\right) = \left(\boldsymbol{\omega}\times\tilde{\boldsymbol{u}}\right). \tag{10}$$

Helmholtz-Hodge Decomposition

Naturally, the incompressibility condition (regarding the concept of a non-radiating base flow of Goldstein) leads to the Helmholtz-Hodge decomposition of the flow field. We propose an additive splitting on the bounded problem domain Ω of the velocity field $\boldsymbol{u}\in\mathrm{L}^2(\Omega)$ in L^2-orthogonal velocity components

$$\boldsymbol{u} = \boldsymbol{u}^{\mathrm{ic}} + \boldsymbol{u}^{\mathrm{c}} + \boldsymbol{u}^{\mathrm{h}} = \nabla\times\boldsymbol{A}^{\mathrm{ic}} + \nabla\phi^{\mathrm{c}} + \boldsymbol{u}^{\mathrm{h}}, \tag{11}$$

where $\boldsymbol{u}^{\mathrm{ic}}$ represents the solenoidal (non-radiating base flow) part, $\boldsymbol{u}^{\mathrm{c}}$ the irrotational (radiating) part and $\boldsymbol{u}^{\mathrm{h}}$ the harmonic (divergence-free and curl-free) part of the flow velocity. The scalar potential ϕ^{c} is associated with the compressible part and the property $\nabla\times\boldsymbol{u}^{\mathrm{c}} = 0$, whereas the vector potential $\boldsymbol{A}^{\mathrm{ic}}$ describes the solenoidal part of the velocity field, satisfying $\nabla\cdot\boldsymbol{u}^{\mathrm{ic}} = 0$.

Based on the decomposition (11) we formulate the actual computation of the additive velocity components for a bounded domain, where the compressible flow field $\boldsymbol{u}$ and its derivatives do not decay towards or vanish at the boundaries of the decomposition domain. Thus, we have to include the harmonic part $\boldsymbol{u}^{\mathrm{h}}$ of the decomposition. The harmonic part is the homogeneous solution of the partial differential equation and physically speaking the potential flow solution of the configuration. The decomposition domain is depicted in Figure 2, with the flow boundaries $\Gamma_{1,\ldots,4}$. Now, we have to be aware that at reentrant corners of the cavity singularities in the compressible velocity component $\boldsymbol{u}^{*,c} = \nabla\phi^{*,c}$ arise. This holds for domains, where corners with an angle $\theta > \pi$ exist. Therefore, instead of solving for the compressible part, we apply the curl to (11) and obtain the vector valued curl-curl equation with the vorticity $\boldsymbol{\omega} = \nabla\times\boldsymbol{u}$ as forcing

$$\nabla\times\nabla\times\boldsymbol{A}^{*,\mathrm{ic}} = \nabla\times\boldsymbol{u} = \boldsymbol{\omega}. \tag{12}$$

The star denotes the joint function of both parts, the incompressible and the harmonic one. The function space $\mathcal{W}$ for the vector potential

$$\mathcal{W} = \left\{\boldsymbol{\varphi}\in H\left(curl,\Omega\right) \middle| \boldsymbol{n}\times\nabla\times\boldsymbol{\varphi} = \boldsymbol{n}\times\boldsymbol{u} \ \text{ on } \ \Gamma_{1,2,3,4}\right\}$$

requires a finite element discretization with edge elements (Nédélec elements) [12]. Due to the space $\mathcal{W}$ and the orthogonality condition, the decomposition fulfills along the boundary

$$\int_{\Gamma} \boldsymbol{A}^{*,\mathrm{ic}}\cdot\left(\boldsymbol{u}^{\mathrm{c}}\times\boldsymbol{n}\right)\mathrm{d}s = 0, \tag{13}$$

ensuring the orthogonality of the components and an unique decomposition. Finally, we obtain the non-radiating component, which contains all divergence-free components, as

$$\tilde{\boldsymbol{u}} := \boldsymbol{u}^{*,\mathrm{ic}} = \nabla\times\boldsymbol{A}^{*,\mathrm{ic}}. \tag{14}$$

Application

We demonstrate the proposed method for the aeroacoustic benchmark case [4], cavity with a lip. The geometrical properties are given in Figure 1, with all spatial dimensions in mm. The deep cavity has a reduced cross-section at the orifice (Helmholtz resonator like geometry) and the cavity separates two flat plate configurations. The Helmholtz resonance of the cavity is at about 4.4 kHz. The flow, with a free-stream velocity of $U_\infty = 50$ m/s, develops over the plate up to a boundary layer thickness of $\delta = 10$ mm. For this configuration we expect the first shear layer mode at about $f_{s1} = 1.7$ kHz.

Fluid Dynamics The unsteady, compressible, and laminar flow simulation is performed with a prescribed velocity profile

FIGURE 1 The geometry and the flow configuration of the benchmark problem, cavity with a lip.

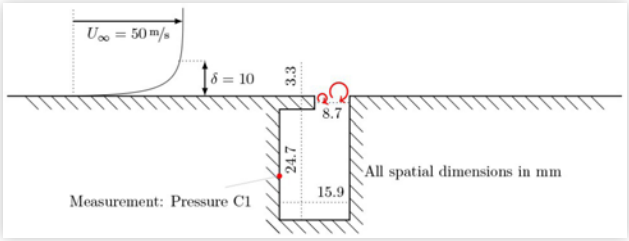

FIGURE 2 The flow domain Ω_F is a subdomain of the acoustic domain Ω_A, which includes the flow domain as its source domain and the propagation domain Ω_P.

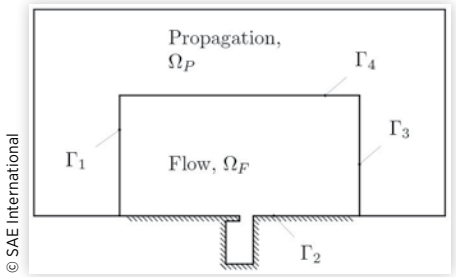

$\boldsymbol{u} = \boldsymbol{u}_{in}$ at the inlet Γ_1, a no slip and no penetration condition $\boldsymbol{u} = \mathbf{0}$ for the wall Γ_2, an enforced reference pressure $p = p_{ref}$ at the outlet Γ_3, and a symmetry condition $\boldsymbol{u} \cdot \boldsymbol{n} = 0$ at the top Γ_4 (see Figure 2). Thereby, the commercial CFD software Ansys-Fluent has been used.

The compressible flow simulation predicts the first shear layer mode at f_{s1} = 1.7 kHz accurately (see Figure 3), which is also confirmed by measurements [13]. An incompressible simulation misinterprets the physics and predicts a shear layer mode of second type [14]. However, Figure 3 also shows a strong peak at 1400 Hz and two minor peaks at around 1150 Hz. The artificial computational domain resonances are excited by compressible effects. This shows how important it is to model boundaries with respect to the physical phenomena.

A direct numerical simulation using a commercial flow solver, resolving flow and acoustic, suffers the following main drawbacks. First, transmission boundaries for vortical and

FIGURE 3 The wall pressure level (WPL) of the compressible flow simulation at the observation point C1 in the cavity. The physical 1st shear layer mode at 1680 Hz and the artificial computational domain resonances are located around 1100 Hz. The reference pressure is 20 μPa.

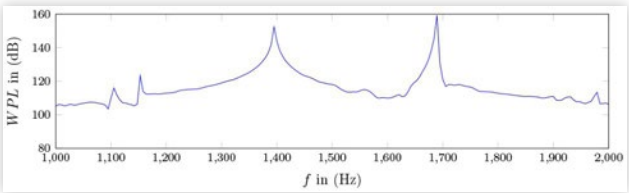

FIGURE 4 The rate of expansion $\nabla \cdot \boldsymbol{u}$ of the compressible flow simulation at a representative time step. The figure demonstrates the presence of standing waves due to the boundary conditions of the compressible flow simulation.

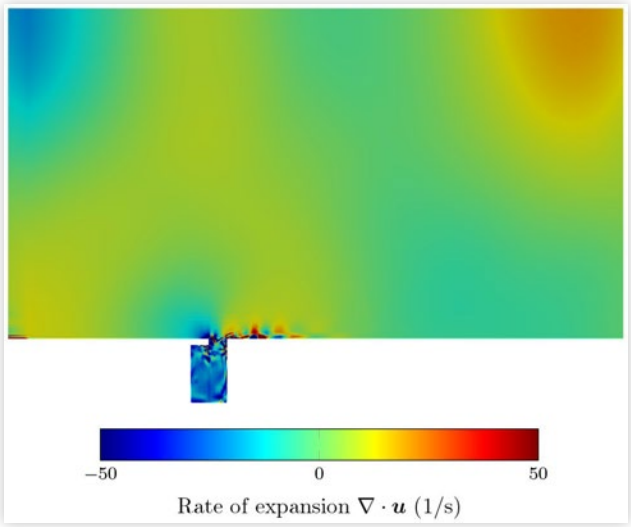

wave structures are limited and often inaccurate. In computational fluid dynamics the boundaries are optimized to propagate vortical structures without reflection. But in contrast to that, the radiation condition of waves are not modeled precisely and, as depicted in Figure 4, artificial computational domain resonances superpose the dominant flow field. The state of the art modeling approach in flow simulation utilizes sponge layer techniques, to damp acoustic waves towards the boundaries, so that they have no influence on the simulation with respect to the wave modeling. Second, low order accuracy of currently available commercial flow simulation tools and the numerical damping dissipates the waves before they are propagated into the far field. Third, a relatively high computational cost to resolve both flow and acoustics exists.

Helmholtz-Hodge Decomposition For each time step of the compressible flow computation, we solve (12) with the appropriate boundary conditions

$$\boldsymbol{n} \times \nabla \times A^{*,ic} = \boldsymbol{n} \times \boldsymbol{u} \quad \text{on} \quad \Gamma_{1,2,3,4}$$

and obtain the vortical velocity field according to (14). As displayed in Figure 5, no singularities at the reentrant corners arise and the overall extracted non-radiating velocity field contains all divergence-free components. This method tackles the compressible phenomena inside the domain Ω_F by filtering the domain artifacts of the compressible flow field such that the computed sources are not corrupted. Figure 6 illustrates the shape and nature of the Lamb vector for a characteristic time step. As one can see, there is almost no visible difference in the source term. Therefore, we have performed a Fourier-transform and display in Figure 7 the x– and y–components of the obtained Lamb vectors in the frequency domain at the first shear layer mode (1660 Hz). Now, the difference in the spatial distribution gets visible.

FIGURE 5 The magnitude of the incompressible component of the flow velocity captures the vortical flow features of the simulation.

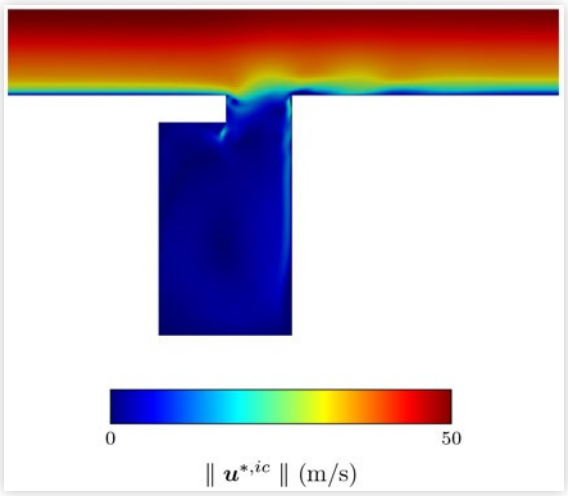

FIGURE 6 Comparison of the Lamb vector for the corrected and the non-corrected calculation.

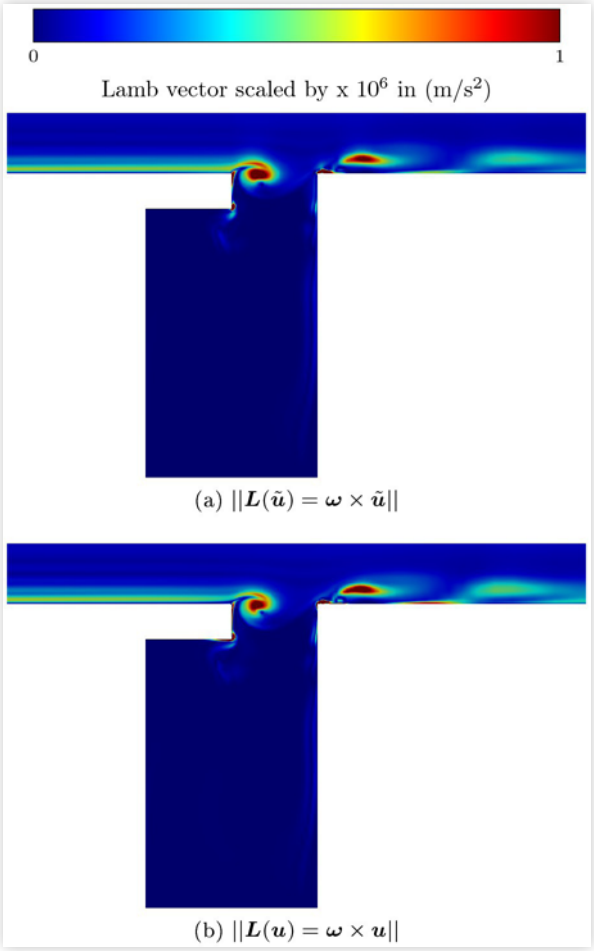

FIGURE 7 Comparison of the Lamb vector for the corrected and the non-corrected calculation at the first shear layer mode.

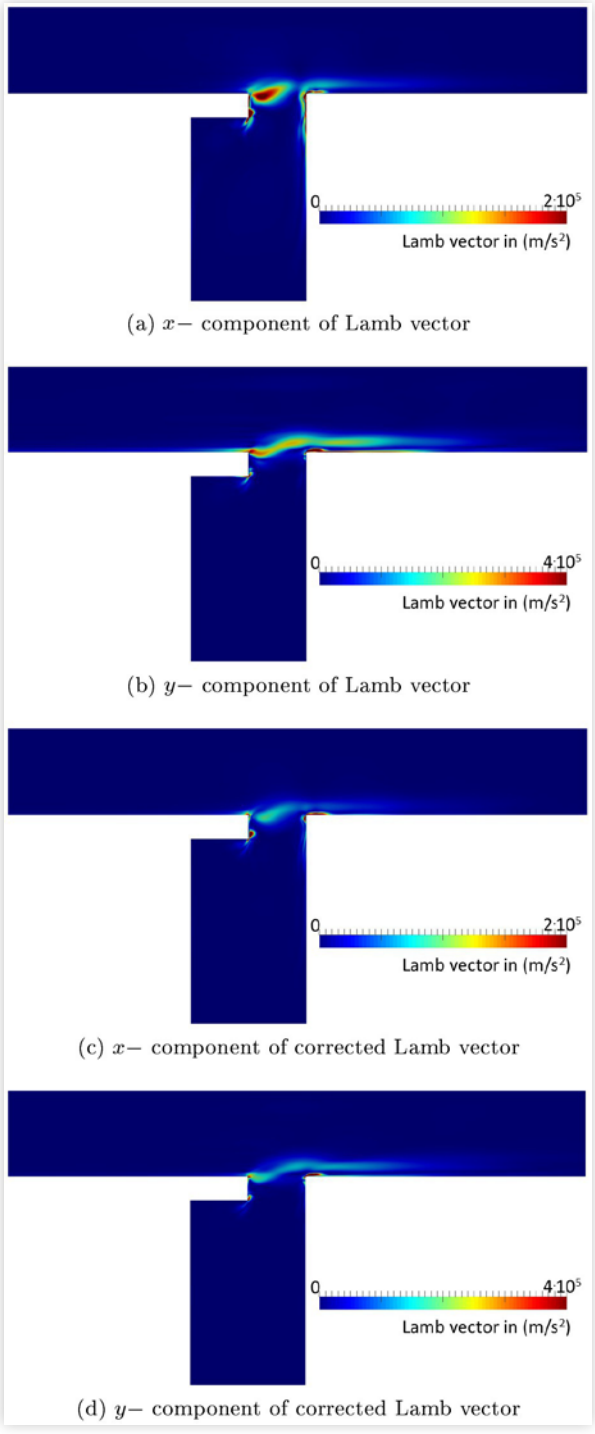

Acoustic Propagation The acoustic simulation utilizes the equation of vortex sound (8) to compute the acoustic propagation applying the finite element method by using the in-house solver CFS++ [12]. The Doppler effect is included in the convective property of the wave operator, upstreams the wavefronts reduce their wavelength and

FIGURE 8 Field of the total enthalpy fluctuation H at a characteristic time. (a) Aeroacoustic sources are due to a compressible flow simulation without applying the correction. (b) Aeroacoustic sources of the wave equation are due to a compressible flow simulation applying the correction.

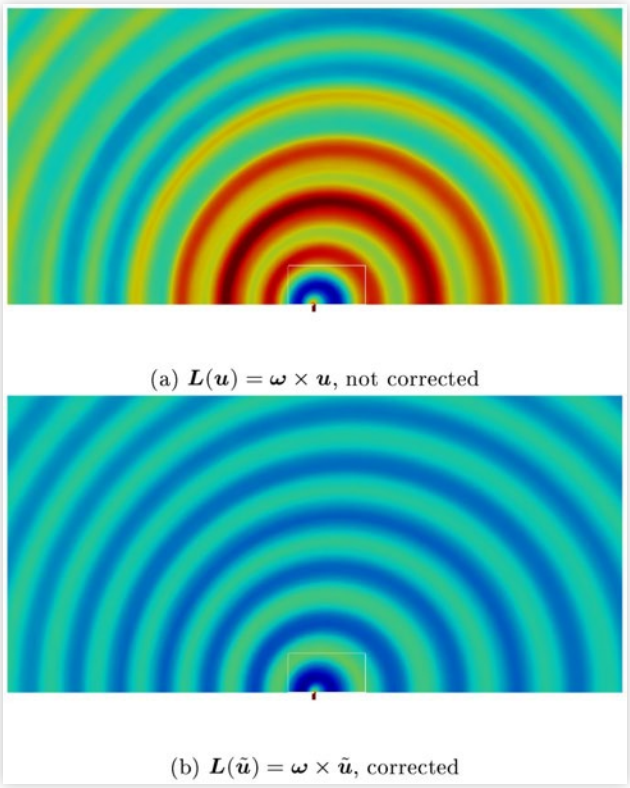

downstream the distance between the peaks of the wavefronts are enlarged. The finite element domain consists of three sub-domains being independently discretized and connected by non-conforming Nitsche-type Mortar interfaces [15]. The acoustic sources are prescribed in the source domain and a final outer perfectly matching layer ensures accurate free field radiation. Two different aeroacoustic source variants are investigated, the uncorrected Lamb vector $\boldsymbol{L}(\boldsymbol{u})$ (field quantities directly from the flow simulation) and the corrected Lamb vector $\boldsymbol{L}(\tilde{\boldsymbol{u}})$ based on the Helmholtz-Hodge decomposition in the vector potential formulation. Figure 8 compares the resulting acoustic fields. As expected, the acoustic field computed by the corrected source term is strongly reduced in amplitude and shows a typically wave propagation, whereas Figure 8a shows perturbations.

The ideal gas law and (7) serves us a relation between the specific enthalpy H and the sound pressure p_a. In its linearized form, $H/R_sT \ll 1$, the sound pressure level (SPL) computes by

$$SPL = 20\log\left(\frac{H}{R_s T p_{a,\mathrm{ref}}}\right) \tag{15}$$

FIGURE 9 Comparison of the SPL level outside the cavity. The spectrum of the corrected Lamb vector formulation reveals that only the shear layer mode is present.

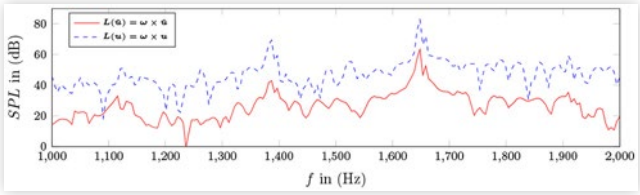

TABLE I Comparison of the pressure outside the cavity

	f_{s1}/Hz	SPL_{s1}/dB
Experiment	1650	30
Simulation $\boldsymbol{L}(\tilde{\boldsymbol{u}}) = \boldsymbol{\omega} \times \tilde{\boldsymbol{u}}$	1660	34
Simulation $\boldsymbol{L}(\boldsymbol{u}) = \boldsymbol{\omega} \times \boldsymbol{u}$	1660	52

with $p_{a,\,\mathrm{ref}}$ being 20 μPa. The plotted sound spectra of the computations in the far field as shown in Figure 9 reveal that the SPL of the non-corrected source terms are much higher. Furthermore, the spectrum obtained by the corrected source term mainly reveals the physical 1st shear layer mode and strongly suppresses all artificial domain resonance modes. Table I quantifies the obtained results in the far field, where the computed 2D acoustic sound pressure has been scaled according to [16] for comparison with the measured data. Thereby, the computations of the non-corrected source terms overestimate the experimental result by 22 dB. In the case of the corrected source terms, the overestimation is just 4 dB. These results strongly demonstrates the applicability of our Helmholtz-Hodge decomposition approach.

Conclusions

According to the resolution of the numerical scheme, a compressible flow simulation already contains wave components. Therefore, the sources of an aeroacoustic analogy have to be filtered such that a non-radiating base flow is obtained from which the source terms are computed. We show that with the help of a Helmholtz-Hodge decomposition, it is possible to extract the vortical (non-radiating) flow component for arbitrary domains. Furthermore, the method filters domain resonant artifacts, which arises due to limited boundary condition treatment in the numerical simulation. As we rely on the divergence free formulation, the equation to obtain the vector potential serves as a valid formulation to extract all divergence-free parts of the flow. The final validation example shows remarkable results for the SPL outside the cavity and the characteristics of the monopole radiation is captured well.

References

1. Hardin, J.C. and Hussaini, M.Y., "Computational Aeroacoustics for Low Mach Number Flows,". In: *Computational Aeroacoustics*. (New York, Springer-Verlag, 1992), 50-68.
2. Wagner, C., Hüttl, T., and Sagaut, P., editors, *Large-Eddy Simulation for Acoustics* (Cambridge University Press, 2007).
3. Kaltenbacher, M., Hüppe, A., Reppenhagen, A., Tautz, M. et al., "Computational Aeroacoustics for HVAC Systems Utilizing a Hybrid Approach," *SAE International* 9:1047-1052, 2016.
4. Henderson, B., "Automobile Noise Involving Feedback-Sound Generation by Low Speed Cavity Flows," Technical report, in Third Computational Aeroacoustic(CAA) Workshop on Benchmark Problems, 2000.
5. Lighthill, M.J., "On Sound Generated Aerodynamically. I. General," *Theory Lond.* A 211:564-587, 1952.
6. Lighthill, M.J., "On Sound Generated Aerodynamically II. Turbulence as a Source of Sound," *Proc. Roy. Soc. Lond.* A 222:1-32, 1954.
7. Phillips, O.M., "On the Generation of Sound by Supersonic Turbulent Shear Layers," *Journal of Fluid Mechanics* 9:1-18, 1960.
8. Lilley, G.M., "On the Noise from Jets," Technical report, AGARD CP-131, 1974.
9. Goldstein, M.E., *Aeroacoustics* (McGraw-Hill, 1976).
10. Goldstein, M.E., "A Generalized Acoustic Analogy," *Journal of Fluid Mechanics* 488:315-333, 2003.
11. Howe, M.S., *Theory of Vortex Sound*. Cambridge Texts in Applied Mathematics, 2003.
12. Kaltenbacher, M., *Numerical Simulation of Mechatronic Sensors and Actuators: Finite Elements for Computational Multiphysics* Third Edition (Springer, 2015).
13. Seitz, T., "Experimentelle Untersuchungen der Schallabstrahlung bei der Überströmung einer Kavität, Master's thesis, Friedrich Alexander Universität Erlangen, 2005.
14. Farkas, B. and Paal, G., "Numerical Study on the Flow over a Simplified Vehicle Door Gap an Old Benchmark Problem Is Revisited," *Period. Polytech. Civil Eng.* 59(3):337-346, 2015.
15. Kaltenbacher, M., Hüppe, A., Grabinger, J., and Wohlmuth, B., "Modeling and Finite Element Formulation for Acoustic Problems Including Rotating Domains," *AIAA Journal* 54:3768-3777, 2016.
16. Oberai, A., Roknaldin, F., and Hughes, T.J.R., "Computation of Trailing-Edge Noise Due to Turbulent Flow over an Airfoil," *AIAA* 40(11):2206-2216, 2002.

ISSN 0148-7191